



Improving physical properties of sodium caseinate based coating with the optimal formulation: Effect on strawberries' respiration and transpiration rates

Nicoletta Antonella Miele, Stefania Volpe, Elena Torrieri^{*}, Silvana Cavella

Department of Agricultural Sciences, Unit of Food Science and Technology - University of Naples Federico II, 80055, Portici, Italy

ARTICLE INFO

Keywords:

Biopolymer coating
Caseinate/guar gum
Wax
Emulsion
Water vapor permeability

ABSTRACT

The objective of the work was to improve the physical properties of caseinate (SC)-based coating by using a thickening agent, guar gum (GG), and a solid fat phase, beeswax (BW). To this aim, the effect of GG, BW, and surfactant concentration, varying the hydrophilic-lipophilic balance (HLB) values given by surfactant combination, on the physicochemical properties of the caseinate-based blends and film has been investigated. The best formulation has been applied to strawberries to quantify the impact of the coating on respiration and transpiration rates. The results showed that GG, BW, their interaction, and HLB affected the physical properties of the sodium caseinate-based coating. The formulations most physically stable and containing small and uniform solid BW particles were those with an HLB of 9.2. GG affected the viscosity of the blends, whereas the effect of beeswax concentration on viscosity was very low. A 50% of reduction of water vapor permeability was obtained by changing GG and BW concentration. The best formulation, containing 8% SC, 0.2% GG, 2% BW, and Tween 80 and Span 80 at HLB of 9.2, was able to reduce the respiration and transpiration rates of strawberries by 17% and 40%, respectively, at 4 °C and relative humidity higher than 86%.

1. Introduction

Edible coatings or films are a promising preservation technology that has shown favorable results in extending the fresh fruits and vegetables (F&V) shelf life (Falguera et al., 2011; Otoni et al., 2017; Khan et al., 2021). Casein and its derivatives have been extensively studied due to their availability, low cost, and complete biodegradability. Sodium caseinate (SC), obtained by acid precipitation of casein, has distinct properties which make them highly suitable for biopolymer films, such as high thermal stability, capability to form micelle, emulsification capability, the ability to bind with small ions and molecules, the water solubility and their high nutritional value (Hernandez-Izquierdo and Krochta, 2008; Khan et al., 2021). Improved mechanical properties can be obtained by blending sodium caseinate with polysaccharides (Perone et al., 2014; Volpe et al., 2017). Moreover, including a hydrophobic lipid compound into the composite material improves the water vapor barrier of the resulting film/coating (Galus and Kadzinska, 2015; Galus et al., 2020). For coating application on F&V, the viscosity is a critical parameter to obtain a coating of adequate thickness and uniformity. Based on the physical principles of a dip-plate coating, rheological

properties of the solution is a critical parameter for coating composition optimization (Cisneros-Zevallos and Krochta, 2003). For sodium caseinate (SC) coating applied on fresh fennel, the thickness of the dry coating ranged between 0.7 and 6.4 μm, respectively, for SC coating with an apparent viscosity between 4×10^{-5} Pa · s and 0.4 Pa · s (Valentino et al., 2020). Recent studies reported that for bio-based suspensions with a shear-thinning behavior, a viscosity value at 1 s^{-1} varying from 0.02 to 2 Pa · s is suitable for obtaining suitable coatings for fruit preservation (Fei et al., 2021; Sun et al., 2021). In addition, for dispersions-based coatings, the suspension stability and the particle size dimension and distribution are additional critical factors affecting the coating's water vapor transmission rate. To prevent instability, droplets must be stabilized by using surfactants both in the emulsion, to prevent coalescence, and in the dispersion, to avoid Ostwald ripening and sedimentation (Lindner et al., 2018). The non-ionic surfactants such as span and tween are widely used for emulsion-based films and coatings (Shamsuri and Siti Nurul, 2020); among them, tween 80, a hydrophilic surfactant, and span 80, a hydrophobic surfactant, are generally used together to reach the hydrophilic-lipophilic balance (HLB) required. Their combination acts as an emulsifier, reducing the interfacial tension

^{*} Corresponding author.

E-mail address: elena.torrieri@unina.it (E. Torrieri).

of each phase and achieving better interfacial packing (Han et al., 2011; Zhang et al., 2019; Lindner et al., 2018). In a candelilla wax emulsion for a coating application, surfactants with HLB values of between 11 and 13.5 produce the lowest particle diameter, a span of volume distribution, and flotation rate of particles (Lindner et al., 2018). In a more recent study, only tween 80 (HLB of 15) was used as a surfactant in sodium caseinate, candelilla and carnauba wax-based films (Galus et al., 2020). Dispersion-based coatings are a very complex system, and their physical properties must be optimized as a function of product requirements.

Among fresh F&V, strawberries are very perishable product due to the high respiration rate and the high susceptibility. Its deterioration causes high depreciation in sales at retailing points (Lafarga et al., 2019). Transpiration rate and respiration rate are the two physiological parameters studied as physiological indicators to properly design a package able to preserve the product quality (Sousa-Gallagher et al., 2013; Bovi et al., 2018). Moreover, by reducing respiration rate and transpiration rate is possible to retard product senescence and, in turn, extend product shelf life (Jalali et al., 2020).

Thus, the objective of the work was to improve the physical properties of caseinate-based coating by using a thickener agent, guar gum, and a solid fat phase, beeswax, to obtain a coating of adequate thickness and with barrier properties able to control the respiration rate and transpiration rate of fresh strawberries. To this aim, the effect of beeswax, guar gum, and surfactant concentration, varying HLB values given by surfactant combination, on the physicochemical properties of the caseinate-based blends has been investigated. The critical parameter affecting coating performance have been investigated, including their viscosity, physical stability, particle size distributions, moisture sorption adsorption behavior, and water vapor permeability of the obtained film. Finally, the best formulation has been applied as a coating to strawberries to study its effect on respiration rate and transpiration rate.

2. Materials and methods

2.1. Materials

Sodium caseinate (SC), glycerol (GLY), tween 80 (T), span 80 (S), and guar gum (GG) were purchased from Sigma-Aldrich & Co. (Milano, Italia). Beeswax was purchased from Agraria Ughetto Apicoltura (Giarvenno, Torino, Italia).

2.2. Preparation of biopolymer blend

SC solution with protein concentrations of 8.0% (weight (w)/volume (v)) was obtained by dispersing SC powder in deionized water and stirring continuously for 1.3 h at 90 °C; GLY was added as a plasticizer to obtain a GLY/SC weight ratio of 0.1. Then GG (0.2% or 0.4% (w/v)) was added under stirring for another 30 min at 90 °C. Next, BW (1% or 2% (w/v)) and surfactants (0-0.5% w/v) at different T/S ratio (0, 1:3, 1:1, 3:1) were added, and the mixture was stirred in a double-walled reactor, for 10 min at 90 °C, to allow the wax to melt. Surfactants were obtained by mixing tween 80 (HLB 15) and span 80 (HLB 4.2), with HLB values between 7, 9.2, and 12.5. The ratio BW:S was constant and equal to 4:1. Emulsification of the hot sample was achieved using an Ultra-Turrax T25 system (IKA-Werke, Staufen im Breisgau, Germany), running at 15,000 rpm for 5 min. The emulsions were stirred at a constant rate of 230 rpm until room temperature was reached so that the wax droplets could solidify. Table 1 reports the composition of the studied samples. The ranges of GG, BW, and surfactant concentrations were selected based on previous studies (Avena-Bustillos and Krochta, 1993; Galus et al., 2020).

2.3. Viscosity

The viscosity was measured using a stress-controlled rheometer

Table 1
Formulations of the analyzed samples.

Samples	Composition				
	T (%)	S (%)	T:S	BW (%)	GG (%)
1 ^a	0	0	0	1	0.2
2 ^a	0	0	0	1	0.4
3 ^a	0	0	0	2	0.2
4 ^a	0	0	0	2	0.4
5 ^b	0.063	0.187	1:3	1	0.2
6 ^b	0.063	0.187	1:3	1	0.4
7 ^b	0.125	0.375	1:3	2	0.2
8 ^b	0.125	0.375	1:3	2	0.4
9 ^c	0.125	0.125	1:1	1	0.2
10 ^c	0.125	0.125	1:1	1	0.4
11 ^c	0.25	0.25	1:1	2	0.2
12 ^c	0.25	0.25	1:1	2	0.4
13 ^d	0.187	0.063	3:1	1	0.2
14 ^d	0.187	0.063	3:1	1	0.4
15 ^d	0.375	0.125	3:1	2	0.2
16 ^d	0.375	0.125	3:1	2	0.4

T: Tween 80; S: Span 80; BW: Beeswax; GG: Guar gum; a: no surfactant; b:HLB: 7; c: HLB = 9.2; d: HLB = 12.5.

(HAAKE MARS 40 Rheometer, Thermo Fisher Scientific, Waltham, MA, USA) equipped with coaxial cylinders (30 mm outer diameter and 26 mm internal diameter). Steady shear tests were carried out at 15 °C by increasing the shear rate from 0.1 to 100 s⁻¹. The experimental apparent viscosity data as a function of shear rate were described by the Cross model (Santos et al., 2016):

$$\eta = \frac{\eta_0}{1 + \left(\frac{\dot{\gamma}}{\dot{\gamma}_c}\right)^{1-n}} \quad (1)$$

where $\dot{\gamma}_c$ is the critical shear rate for the onset of shear-thinning behavior, η_0 stands for the zero-shear viscosity, and n is the flow index. Optimal viscosity values for coating application must be in the range of 0.2–2 Pa · s (Fei et al., 2021; Sun et al., 2021).

2.4. Particle size distribution

The particle size distribution (PSD) was analyzed by using a laser diffraction particle size analyzer (Mastersizer, Malvern Instruments, Worcestershire, UK) equipped with a Hydro 3000 dispersion unit at 25 °C (dispersant medium: water; lens arrangement: reverse Fourier; laser obscuration: 3–20%, depending on particle size dimension; refractive indexes for the dispersant and the dispersed phases respectively: 1.33 and 1.55). About 0.1 g of each sample was analyzed as such. For each dispersion, two different replicates were analyzed and for each replicate, 5–10 measurements were performed. The Sauter diameter $d_{3,2}$, and De Brouckere diameter $d_{4,3}$ has been determined. Furthermore, the widths of the volume and number distribution, referred to as span and uniformity, respectively, were used to evaluate the polydispersity of the particles. The criteria for samples selection for coating application were the lowest diameter of particle and the lowest polydispersity.

2.5. Physical stability

The sample's stability of all samples was evaluated by measuring the backscattering (BS) of pulsed near-infrared light (wavelength of 880 nm) using a Turbiscan Tower stability analyzer (Formulation, France). Dispersions were placed into cylindrical glass tubes up to the height of 45 mm and scanned for 16 h at 30 °C to accelerate destabilization kinetics. The stability of samples was expressed using the Turbiscan Stability Index (TSI), which is defined as follow:

$$TSI = \frac{\sum_i \sum_h |scan_i(h) - scan_{i-1}(h)|}{N_h} \quad (2)$$

where scan_i (h) is the light intensity of the scan acquired at the i -th time instant and a height of h , and N_h is the number of height positions in the selected scanning zone of the tube (top, centre, bottom or global) (Cavella et al., 2020). TSI is a dimensionless number resulting by summing all occurring destabilization phenomena in the sample (sedimentation, flocculation, aggregation, and creaming). The higher the TSI value, the lower the stability. A TSI <1.5 was the criteria for optimization.

2.6. Film-making procedure

Based on the previous criteria for optimization, formulations 9, 10, 11, and 12 were used to prepare films by casting. A volume of 5 ml of each blend was poured into Petri dishes (area = 56.7 cm²) and placed in a circulating air system chamber (MMM Group, Planegg, Germany) at 30 °C and 50% RH overnight to allow the drying.

2.7. Color, thickness, and moisture content

The film's color was determined as reported by Volpe et al. (2017) using a colorimeter (Minolta Chroma Meter, CR 300, Japan). The Hunter parameters L* (from 0 = black to 100 = white), a* (-a* = greenness to +a* = redness), and b* (-b* = blueness to +b* = yellowness) were measured and averaged from random positions of each film. Film thickness was measured using a micrometer model H062 with a sensitivity of ±2 μm (Metrocontrol Srl, Casoria, NA, Italy). Five replications were conducted for each sample treatment. Five measurements were taken at random positions around the film sample.

2.8. Water vapor permeability

The water vapor permeability (WVP) of the films was evaluated as reported by Volpe et al. (2017) using a gravimetric test according to ASTM E 96 (1993) by means of Payne permeability cup (Carlo Erba, Milan, Italy). The Water vapor permeability (WVP) was calculated at 20 °C and at 85% of RH, as:

$$WVP = \frac{x}{(A \cdot \Delta p)} \cdot \frac{dm}{dt} \quad (3)$$

Where "dm/dt" is the slope of the weight curve with respect to time after reaching the steady-state, "x" is the thickness, "A" is the exposed area of the film (9.89 cm²), "Δp" is the difference of water vapor pressure through the film. Assuming that the pressure of the steam inside the cups is equal to zero, due to the presence of silica gel, Δp is equal to the pressure of the water vapor inside the dryer.

The criterion for coating selection was the lowest WVP.

2.9. Adsorption isotherm

The adsorption isotherm of films was determined by using a microbalance system (DVS dynamic vapor sorption Q500SA, TA Instrument, New Castle, USA). The desired relative humidity (RH) was obtained by mixing dry nitrogen with water vapor saturated nitrogen in determined proportions. The microbalance system allowed the measurement of the mass variation due to the uptake of water with an accuracy of 0.1 mg. Film samples of about 1–2 mg were placed in aluminum cups, whereas as a reference an empty aluminum cup was used. Each sample was conditioned at 0% RH for an adequate time to achieve a constant weight and then RH increased in steps from 5% to 95%. Film samples remained in each step until the constant weight was reached (change of weight <0.001% for 10 min). Measurements were conducted at 30 °C. The equilibrium moisture content has been reported versus the water activity.

The recognized Guggenheim-Anderson-deBoer (GAB) equation (Eq. (4)) was employed to fit the experimental data. This model was

explained and rearranged as given below:

$$X = \frac{m_0 \times C \times a_w}{(1 - K \times a_w) \times (1 - K \times a_w + C \times K \times a_w)} \quad (4)$$

where m_0 is the monolayer moisture content, a_w is the water activity, C and K are model constants (Villalobos et al., 2006).

2.10. Coating application and thickness estimation

Fresh strawberries fruit (var. Murano) harvested at the commercial maturity stage were purchased from a local supermarket (Sole 365) and stored at 4 °C before the test. Strawberries were qualitatively selected based on color, size, and absence of defects to obtain a homogeneous batch. Among formulations 9, 10, 11, and 12, formulation 11 was selected for coating the strawberries. Each strawberry was dipped in the coating dispersion for 2 min, then drained and finally dried. Fruits were stored at test temperature for approximately 1 h to equilibrium to the temperature before experiments.

To estimate the thickness of the coating on the product, the approach reported by Valentino et al. (2020) has been followed. Considering a truncated cone geometry for the strawberries, and taking into account that the surface tension force is surpassed by the viscous and gravity forces, the average liquid thickness (h_{avg}) has been estimated as follows:

$$h_{avg} = \frac{q}{A} = \frac{2}{3} K \left(\frac{\eta Z}{\rho g t} \right)^{1/2} \quad (5)$$

where q was the coating volume (cm³), A is the surface area of the strawberries (cm²), η is the viscosity of the coating solution, Z is the height of the strawberries (cm), ρ is the solution density, g is the gravitational acceleration, t is the draining time and K is the dimensionless flow factor that can be experimentally determined by linear regression of eq. (5) (Cisneros-Zevallos and Krochta, 2003).

The dry film thickness (H_{avg} , μm) on strawberries at a given draining time has been estimated as function of dry coating load (D_c , g cm⁻²) and calculated as:

$$H_{avg} = \frac{D_c}{\rho_f} \cdot 10 \quad (6)$$

$$D_c = \rho c h_{avg} 1000 \quad (7)$$

where ρ is the coating solution density (g cm⁻³), c is the concentration of solids in solution (g g⁻¹), ρ_f is the dry film density (g cm⁻³).

2.11. Transpiration rate and respiration rate measurements

To evaluate the transpiration rate, a weight loss technique as reported by (Volpe et al., 2018) was used. Strawberries of approximately 14–20 g were placed separately in petri-dishes in jars. Relative humidity within the jars was controlled by using saturated salt solutions of sodium chloride, potassium chloride and potassium nitrate and pure water giving 76%, 86%, 96% and 100% RH, respectively. The weight loss was measured daily for 7 days using an analytical balance (Kern ADB 200–4, Kern & Sohn GmbH, Balingen, Germany). Transpiration rate (TR) was calculated from the changes in weight of strawberry over time:

$$TR = \frac{M_i - M}{t \times \left(\frac{M_i}{1000} \right)} \quad (8)$$

where TR is the transpiration rate in g kg⁻¹ h⁻¹, M_i and M are the initial weight (g) and the weight of strawberry (g) at time t (h). As a control, strawberries without coating were used.

The respiration rate was measured as reported by Volpe et al. (2019) in a modified closed system. Strawberries (0.25 kg) were placed in steel jars and equilibrated at temperature test (4 °C) prior start the test. The free volume (V_f) was calculated as follow:

$$V_f = V - \frac{W}{\rho} \quad (9)$$

Where V is the volume of jar (4000 ml), W and ρ are the weight (kg) and the apparent density of strawberries (600 kg m^{-3}), respectively. RO_2 was calculated as follows:

$$R_{O_2} = \left(\frac{dy O_2}{dt} \right) \times \left(\frac{V_f}{W} \right) \times \frac{1}{100} \quad (10)$$

2.12. Experimental design and data analysis

To study the effect of surfactant, GG and BW on physicochemical properties of firm forming solution, a full factorial design was used. The surfactant's levels were four; the GG level were two; the BW levels were two (Table 1). Three replicates were performed for each experiment for a total of 48 samples.

The effect of film composition (four levels) on the physical properties of the film was studied. Three replicates were performed for each experiment for a total of 12 samples. The effect of coating and relative humidity on the transpiration rate of strawberries has been studied by factorial design. Two were the levels of coating (absent/presence (the optimal formulation)), and four the levels of relative humidity (76%; 86%; 96%; 100%). Three replicates were performed for each experiment for a total of 24 samples. The effect of coating on respiration rate was studied by t -test. The results are reported as the average of replications of each sample and the results are expressed as mean \pm standard deviation. Data were analyzed using variance by means in SPSS v17.0 for

Windows (SPSS, Milan, Italy). Duncan's test was carried out to find the source of the significant differences within the samples examined. Significant differences were defined at $p < 0.05$.

Fitting of the rheological models was carried out by using the Table curve 2D v 5.01 Systat software Inc, 2002. Different parameters of PSD were estimated by Malvern software. The stability data were analyzed by using the software package TowerSoft Ver 1.2 (Formulation, France).

The root-mean-square error (RMSE) has been used as the indicator for the accuracy of the fit of the model reported in equation (6):

$$RMSE = \sqrt{\frac{\sum (M_e - M_p)^2}{n}} \quad (11)$$

where M_e is the experimental value, M_p is the predicted value, and n is the number of data points.

3. Results & discussion

3.1. Film forming blend characterization

3.1.1. Particle size distribution (PSD)

The dispersions-based coatings properties depend on the particle size of the dispersed phase: small particle sizes with a narrow distribution are required to obtain stable dispersion and coating with a continuous structure and enhanced barrier properties (Galus and Kadzinska, 2015). Fig. 1 shows the effect of the coating composition on particle size distribution. Samples without surfactants presented three different particle

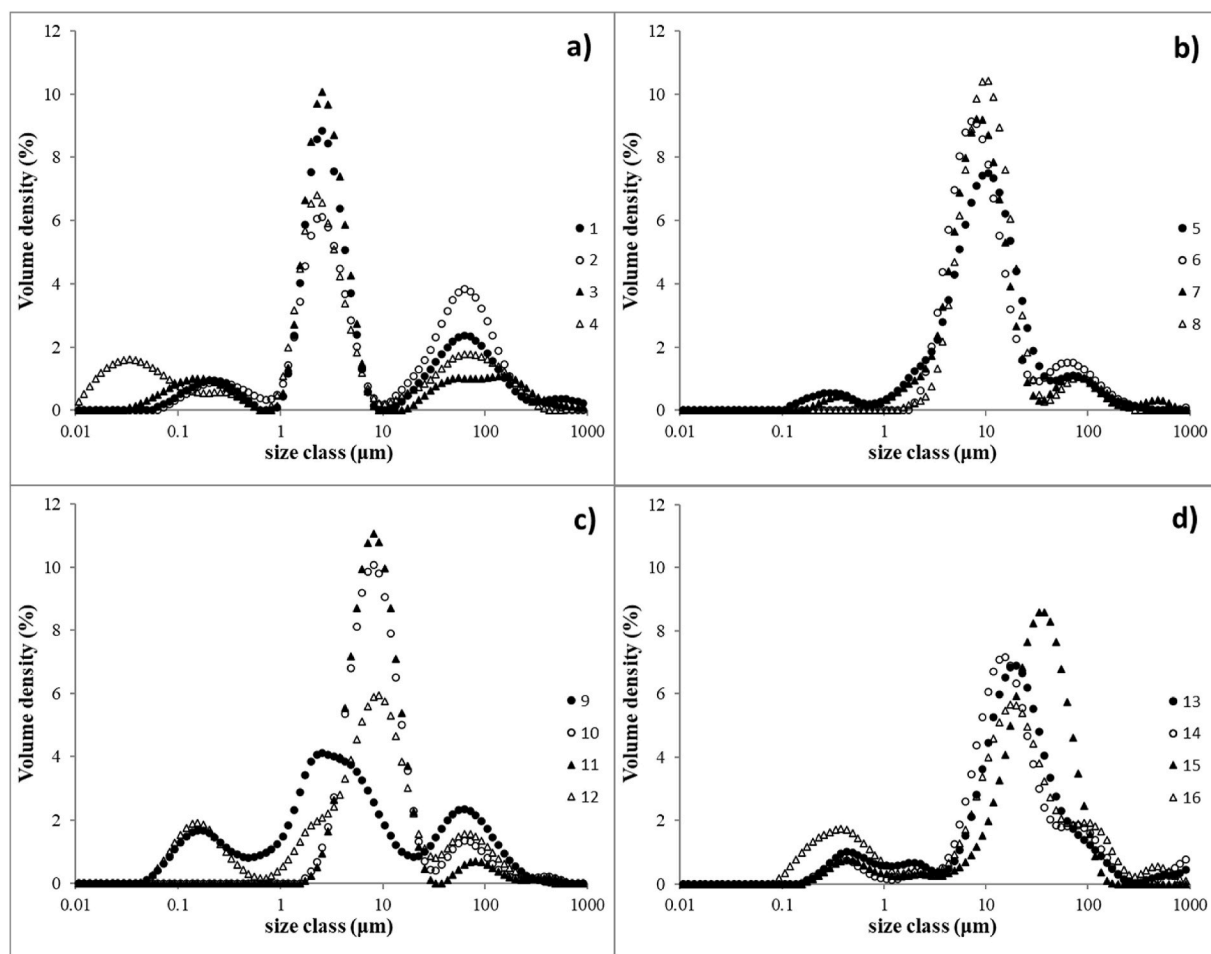


Fig. 1. Particle size distributions of 16 formulations. a) formulations 1–4, without surfactants; b) formulations, with surfactants HLB 7; c) formulations 9–12, with surfactants HLB 9.2; d) formulations 13–16, with surfactants, HLB 12.5.

populations in a wide range of particle sizes (0.01–1000 μm) (Fig. 1 a). The inclusion of surfactants (Fig. 1 b-c-d) reduced the particle size range (0.1–1000 μm). Most of the wax particles are in the same particle size range, except those reported in Fig. 1d. Overall, PDS curves mainly differ for the presence of smaller and bigger particles, depending on formula composition. Those results underline the difficulty of obtaining a homogeneous dispersion with a rotor-stator homogenizer (Galus et al., 2020). The right HLB based on wax and gum formula content seems to be crucial. To better compare samples for their granulometric characteristics, in Table 2 the sample granulometric characteristics, in terms of $d_{[4,3]}$, $d_{[3,2]}$, span, and uniformity are reported. The value of $d_{[4,3]}$ varied a lot among formulations, from a minimum of 13 μm , for a formulation with an HLB of 9.2 (sample 11), to a maximum of 112 μm , for a formulation with an HLB of 12.5 (sample 13). However, ANOVA results highlighted no significant difference among samples 1 to 12, which assumed an average value of $d_{[4,3]}$ of 23,15 μm , whereas a wide variability was observed among samples 13, 14, 15, and 16, which had an HLB of 12.5. On the contrary, The PSD parameters $d_{[3,2]}$ changed from 0.149 to 9.117 μm , but there is not a clear effect of formulation. The inclusion of surfactants significantly reduced span and uniformity values. Only samples with an HLB of 7 and 9.2 (samples 5–12) presented very uniform and small particles. At fixed HLB, the PSD properties depended on the GG and BW concentration. In fact, among samples with HLB of 9.2, sample 9, having 0.2% of GG and 1% of BW, showed the highest value of span and uniformity, whereas sample 11, containing 0.2% of GG and 2% of BW, showed the lowest value of span and uniformity. Thus, only samples 5, 6, 7, 8, 10, 11, and 12 have suitable properties for coating application.

These results reflect that the PSD of an emulsion depends on several formulation-related parameters (McClements, 2007), and even if it could be predicted to a certain extent (Domian and Szczepaniak, 2020), for complex systems, a deeper investigation is needed. For systems containing sodium caseinate, beeswax, and gum, surfactants should be included, because only sodium caseinate, even if it was reported its emulsifying properties (Ma and Chatterton, 2021), was not able to obtain small particles and a narrow particle size distribution (samples 1–4). Small amphiphilic anionic molecules (SAAM) tend to reduce the particle size of the droplets in an emulsion, because they are rapidly adsorbed onto the oil interface, and should prevent droplet re-coalescence. Tween 80 and span 80 are surfactants used for emulsion-based films (Shamsuri and Siti Nurul, 2020) and are both SMAAM, but with a different HLB, which reflects their solubility in the continuous phase and affinity for the droplets, so their usage depends on the system's properties (Espitia et al., 2019). In our study, they were used in combination because, as reported in the literature, it is better to combine two or more surfactants to reach a specific HLB than only one

(Hong et al., 2018).

Galus et al. (2020) reported that in a caseinate-based solution without a thickener agent, a bimodal distribution for candelilla and carnauba wax was observed, in the range of 3–13 μm . By including tween 80 in the system, a reduction of 50% in particle size (d_{90} and d_{50}) has been observed. However, it is important to reduce the particle size but also to improve the uniformity of the particles, reduce the coalescence phenomenon or Ostwald ripening over time, and improve emulsion stability. If the solid particles inside a film-forming solution are quite big and polydisperse, the resulting film and/or coating will be probably heterogeneous, with a negative impact on its barrier properties (Hopkins et al., 2015; Perone et al., 2014b).

Our results highlighted that particle size reduction of the droplets is also affected by the continuous phase characteristics. Gum inclusion should decrease the average droplet diameter and polydispersity (Krstonošić et al., 2015). However, non-ionic gums, such as guar gum, are unable to electrostatically interact with sodium caseinate due to the absence of charge but can be added to improve emulsion stability (Ma and Chatterton, 2021). In our case, the best guar gum concentration depends also on the amount of fat phase for a specific HLB value.

3.1.2. Viscosity

Fig. 2 shows the viscosity curves of all the 16 samples, divided into 4 groups considering HLB values. For film-forming blends without surfactant (1a), increasing the guar gum concentration from 0.2% to 0.4% corresponded to a higher zero shear rate viscosity, a narrower Newtonian zone, and a greater effect of the shear rate on the viscosity. Similar behavior has been observed also for the samples with surfactants with HLB 7 (1 b), and 12.5 (1 d), with samples with the highest guar gum concentrations being more viscous than the others. The effect of beeswax concentration on viscosity was very low. Viscosity curves of samples 7 and 9 showed that aggregation/disaggregation phenomena can occur at a specific shear rate. Blending the caseinate with another polymer, such as high methoxyl pectin (Jahromi et al., 2020) or chitosan (Volpe et al., 2017), determined a transition from Newtonian to shear-thinning flow behavior. In our systems, the GG caused the same transition. In fact, all the samples showed a non-Newtonian behavior, explained by the role of the guar gum: it worked as a thickener to increase the viscosity of the aqueous phase, forming a strong network.

Cross model well describes the rheological behavior of all the samples, and estimated parameters are reported in Table 3, with a very high R^2 . The highest η_0 value was observed for the sample 16, containing 0.4% of guar gum, 2% of beeswax and an HLB value of 12.5, followed by formulation 12 with the same concentrations of both guar gum and beeswax but different HLB (9); meanwhile, the lowest values corresponded to formulations with the 0.2% of guar gum and 1% of beeswax, with and without surfactants. The parameter $\dot{\gamma}_c$ seemed to be affected by the beeswax content, but only for the formulations containing 0.2% of guar gum. For those formulations, at the lowest beeswax concentrations corresponded formulations with the highest $\dot{\gamma}_c$ values for which a more evident Newtonian behavior was observed. Suspensions with an HLB of 9.2 (samples 9–12) presented comparable $\dot{\gamma}_c$ values. Flow index (n) did not vary a lot among formulations.

3.1.3. Physical stability

In Fig. 3, the physical stability in terms of TSI global over 16 h of the different formulations is reported. Results showed that formulations with the lowest gum concentrations (0.2%) were more stable than the other ones with 0.4% of gum, with TSI value ≈ 1 during 16 h, with the exception of the samples with HLB value equal to 9.2. These samples (9-10-11-12) were equally stable with no guar gum or beeswax concentration effect. This result can be explained considering that in an aqueous medium, guar gum and sodium caseinate showed limited compatibility and had a demixing tendency at higher concentrations, resulting in a protein-rich and a polysaccharide-rich phase (Neirynek et al., 2007). Thus, an excess of guar gum content resulted in a demixing

Table 2
PSD parameters estimated from 16 samples.

Samples	$d_{[4,3]}$ (μm)	$d_{[3,2]}$ (μm)	Uniformity	Span
*beeswax	3.95	1.69	0.832	2.72
1	34.430 ^{abc}	1.294 ^c	10.185 ^{cd}	27.763 ^c
2	33.600 ^{abc}	1.143 ^{bc}	12.461 ^d	34.889 ^e
3	26.233 ^{ab}	0.809 ^c	8.669 ^{cd}	33.022 ^{de}
4	23.267 ^{ab}	0.149 ^a	9.093 ^{cd}	30.395 ^{cd}
5	18.810 ^{ab}	4.247 ^{de}	1.368 ^a	3.313 ^a
6	20.589 ^{ab}	7.902 ^h	1.667 ^a	5.732 ^a
7	22.980 ^{ab}	4.416 ^c	2.071 ^a	3.570 ^a
8	18.700 ^{ab}	9.117 ⁱ	1.117 ^a	2.090 ^a
9	26.167 ^{ab}	0.711 ^b	6.261 ^b	19.855 ^b
10	19.190 ^{ab}	7.648 ^{gh}	1.559 ^a	3.947 ^a
11	13.650 ^a	7.275 ^g	0.966 ^a	1.533 ^a
12	20.243 ^{ab}	1.277 ^c	1.510 ^a	4.137 ^a
13	112.525 ^e	3.889 ^d	5.334 ^b	5.797 ^a
14	48.400 ^{cd}	4.606 ^e	2.284 ^a	4.557 ^a
15	35.590 ^{bc}	5.161 ^f	0.623 ^a	2.047 ^a
16	54.767 ^d	1.375 ^c	2.991 ^a	6.442 ^a

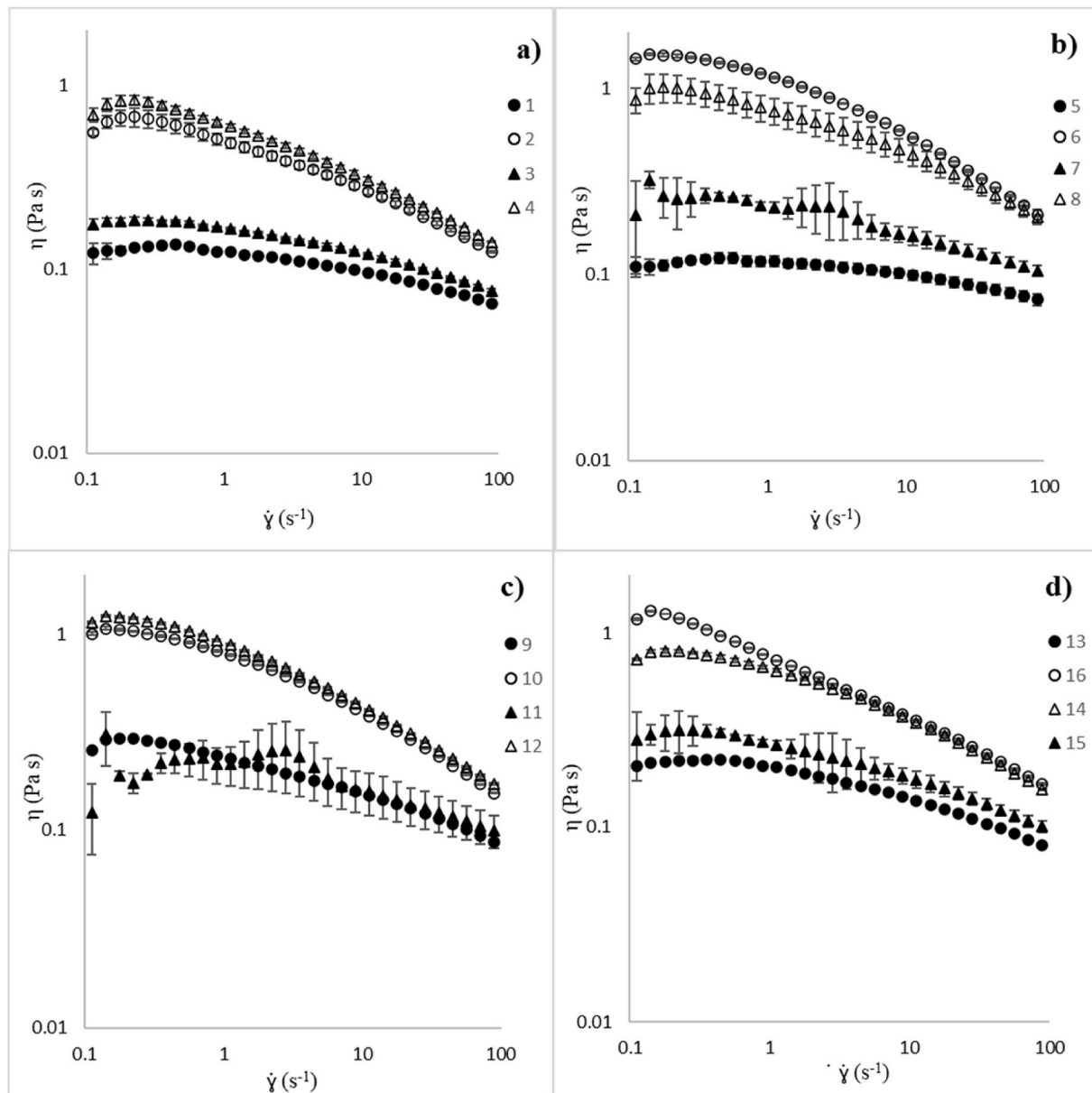


Fig. 2. Apparent viscosity vs shear rate. a) formulations 1–4, without surfactants; b) formulations, with surfactants HLB 7; c) formulations 9–12, with surfactants HLB 9.2; d) formulations 13–16, with surfactants, HLB 12.5.

tendency of the formulation (Neiryneck et al., 2007). However, different destabilization mechanisms will occur in an emulsion system, considering biopolymer compatibility, oil phase content and surfactants (Ma and Chatterton, 2021). In fact, the right choice of the HLB value was the most important parameter affecting the stability of an emulsion system. Moreover, results showed that stability is less affected by the particle size distribution, even if it is known that a smaller particle size emulsion usually meant better physical stability in film-forming solutions (Martin et al., 2018). Thus, TSI results seem to be not highly correlated with PSD, but it is possible that for some systems phenomena of re-coalescence have taken place during dispersion cooling and were not revealed by this analysis, but mainly by PSD results. In conclusion, based on the results, samples with an HLB of 9.2 were selected for their physical stability and their optimal PSD properties (narrow and small particle size distribution of the fat phase). Those samples were used to prepare films.

3.2. Film properties

3.2.1. Color, thickness and moisture content

The optical property of a film is an important quality factor; it can affect the consumer acceptability and the appearance of a product. Table 4 shows the color properties (L^* , a^* and b^*) of the films. No significant differences ($p < 0.05$) were observed for the parameter L^* . The colorimetric parameters a^* and b^* are affected by the concentrations of GG and BW; in particular, the value of a^* significantly increased ($p < 0.05$) from a value of 0.83 ± 0.03 to 1.88 ± 0.01 , suggesting that the more concentration of GG and BW there is, the greener films become. Also, the colorimetric parameter b^* increased with the increase in GG and BW, ranging from a value of 5.6 ± 0.2 to 8.9 ± 0.1 , leading to a more yellow film. The total color difference (ΔE) increased from sample 9 to 12; in particular, with higher concentration of wax, greater total color differences were observed. Similar results were reported by Muscat et al. (2013) for high-amylose starch films prepared with beeswax and carnauba wax. Also, Galus et al. (2020) found that the incorporation of

Table 3

Mean (\pm standard deviations) of η_0 , $\dot{\gamma}_c$, and n values estimated from 16 samples and R2 of the model.

Samples	η_0 (Pa s)	$\dot{\gamma}_c$ (s ⁻¹)	n	R ²
1	0.14 \pm 0.01 ^A	60.94 \pm 9.11 ^D	0.49 \pm 0.10 ^A	0.96 \pm 0.03
2	0.77 \pm 0.07 ^{DE}	3.44 \pm 0.36 ^A	0.47 \pm 0.02 ^A	0.98 \pm 0.01
3	0.20 \pm 0.02 ^{AB}	27.78 \pm 11.58 ^C	0.54 \pm 0.05 ^{AB}	0.99 \pm 0.00
4	0.96 \pm 0.09 ^F	3.07 \pm 0.03 ^A	0.44 \pm 0.03 ^A	0.98 \pm 0.01
5	0.13 \pm 0.02 ^A	100 \pm 0.00 ^E	0.45 \pm 0.32 ^A	0.83 \pm 0.07
6	1.74 \pm 0.04 ^I	3.27 \pm 0.09 ^A	0.38 \pm 0.01 ^A	0.99 \pm 0.00
7	0.58 \pm 0.11 ^C	0.28 \pm 0.30 ^A	0.74 \pm 0.02 ^B	0.98 \pm 0.01
8	1.18 \pm 0.19 ^G	4.05 \pm 1.16 ^A	0.50 \pm 0.04 ^A	0.99 \pm 0.00
9	0.36 \pm 0.00 ^B	5.32 \pm 0.72 ^A	0.59 \pm 0.02 ^{AB}	0.98 \pm 0.00
10	1.28 \pm 0.00 ^{GH}	3.05 \pm 0.07 ^A	0.57 \pm 0.00 ^{AB}	0.99 \pm 0.00
11	0.27 \pm 0.00 ^{AB}	4.37 \pm 0.00 ^A	0.69 \pm 0.00 ^{AB}	0.98 \pm 0.00
12	1.48 \pm 0.05 ^H	2.74 \pm 0.21 ^A	0.43 \pm 0.01 ^A	0.99 \pm 0.00
13	0.24 \pm 0.00 ^{AB}	21.69 \pm 1.48 ^{BC}	0.46 \pm 0.02 ^A	0.98 \pm 0.00
14	0.91 \pm 0.02 ^{EF}	4.95 \pm 0.15 ^A	0.43 \pm 0.01 ^A	0.99 \pm 0.00
15	0.35 \pm 0.02 ^B	11.79 \pm 2.38 ^{BA}	0.52 \pm 0.00 ^{AB}	0.98 \pm 0.01
16	2.44 \pm 0.15 ^J	0.16 \pm 0.04 ^A	0.58 \pm 0.01 ^{AB}	0.99 \pm 0.00

waxe affected the ΔE parameter.

Film thickness values are reported in Table 4 it assumed the value of 0.036 ± 0.005 mm and 0.081 ± 0.005 mm, respectively, for the film with the lowest concentration of GG (0.2%) and BW (1%) and the highest concentration of GG (0.4%) and BW (2%). In agreement with

previous results (Giancone et al., 2008; Perone, Torrieri, Cavella and Masi, 2014; Volpe et al., 2017; Valentino et al., 2020), the thickness is mainly affected by the solid surface content. Thus, as the GG and BW increased, the thickness increased. Its effect is weaker at higher concentrations of wax and gum. The thickness of sample 9 is very similar to those found by Valentino et al. (2020) for the only SC at 8%. The moisture content of films, equilibrated at 50% of RH, changed from a minimum of 7% to a maximum of 8.7% as function of composition. Samples with high concentration of BW showed the lowest moisture content.

3.2.2. Water vapor permeability

The water vapor transmission rate (WVTR) and water vapor permeability (WVP) values are reported in Table 4. No significant differences ($p < 0.05$) were observed in terms of WVTR for samples 10, 11, and 12, which assumed an average value of 73 ± 16 g m⁻² day⁻¹. Sample 9 had the highest WVTR value, equal to 166 ± 0.4 g m⁻² day⁻¹. Comparing the films in terms of WVP, samples 10 and 11 had better water vapor barrier which assumed an average value of $3 \times 10^{-11} \pm 0.8 \times 10^{-11}$. Sample 9 showed the highest value, equal to $7.0 \times 10^{-11} \pm 0.3 \times 10^{-11}$ g m⁻¹ sec⁻¹ Pa⁻¹. This result showed that although BW concentration usually plays a fundamental role in the reduction of water permeability, due to its hydrophobicity, for a complex system the water vapor permeability does not depends only on the hydrophobicity of the

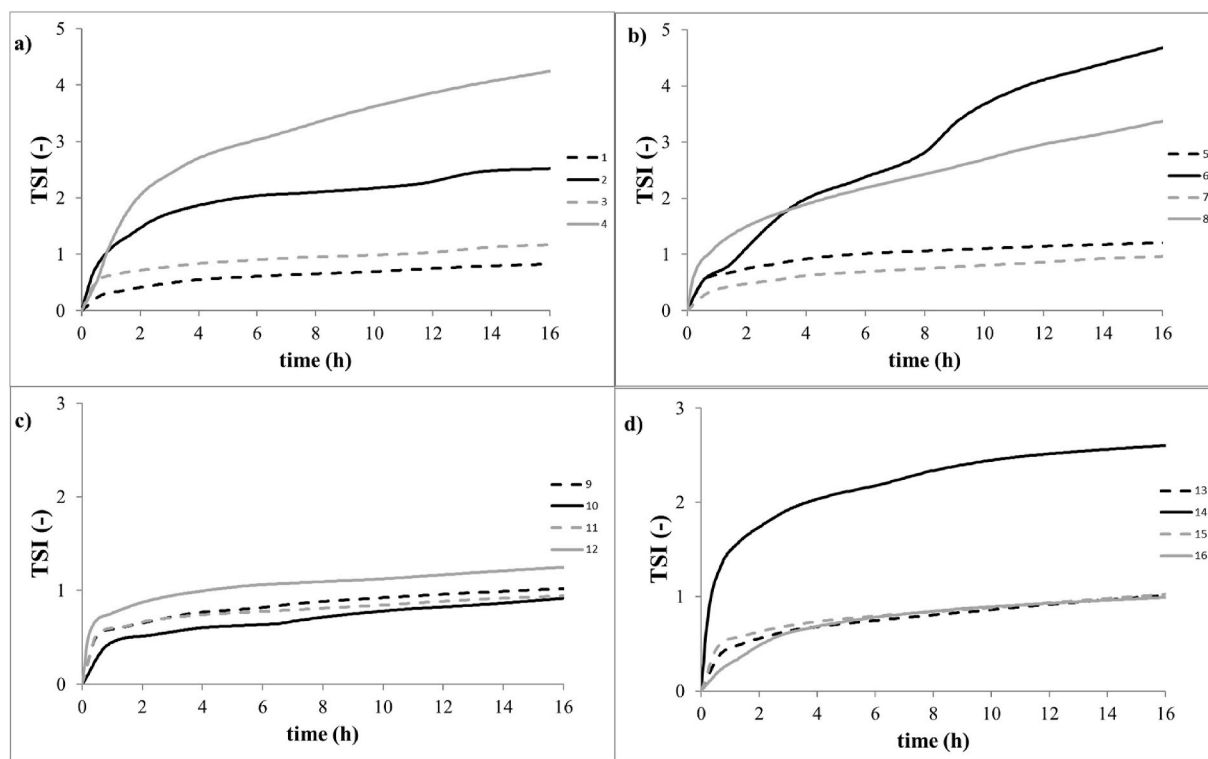


Fig. 3. Global Turbiscan stability index (TSI) vs time. a) formulations 1–4, without surfactants; b) formulations, with surfactants HLB 7; c) formulations 9–12, with surfactants HLB 9.2; d) formulations 13–16, with surfactants, HLB 12.5.

Table 4

Colorimetric parameters (L^a , a^a , b^a , ΔE), thickness, moisture content (MC) and water vapor barrier properties of films obtained from samples 9, 10, 11 and 12.

Samples	L^a	a^a	b^a	ΔE	Thickness (mm)	^a MC %	WVTR (g m ⁻² day ⁻¹)	WVP ($\times 10^{-11}$) (g m ⁻¹ sec ⁻¹ Pa ⁻¹)
9	95.6 \pm 0.3 ^b	0.83 \pm 0.03 ^d	5.6 \pm 0.2 ^a	4.2 \pm 0.9	0.036 \pm 0.005 ^a	8.7	166 \pm 14 ^b	7.0 \pm 0.3 ^c
10	95.1 \pm 0.2 ^a	1.15 \pm 0.07 ^c	6.7 \pm 0.1 ^b	5.4 \pm 0.6	0.076 \pm 0.005 ^b	8.4	59 \pm 17 ^a	2.7 \pm 0.7 ^a
11	95.2 \pm 0.5 ^{ab}	1.43 \pm 0.07 ^b	8.2 \pm 0.2 ^c	7 \pm 1	0.068 \pm 0.005 ^c	7	75 \pm 17 ^a	3.4 \pm 0.9 ^{ab}
12	95.61 \pm 0.06 ^b	1.88 \pm 0.01 ^a	8.9 \pm 0.1 ^d	7.5 \pm 0.7	0.081 \pm 0.005 ^d	7	86 \pm 15 ^a	4.1 \pm 0.6 ^b

^a Measured after equilibrium at 50% of relative humidity.

used additive. It depends on the structure of the film which is a function of the interaction among all the components. At a low percentage of BW in combination with a low percentage of GG (sample 9) the barrier properties of the film were very high, and like that of the film obtained with only sodium caseinate at 8%, prepared in the same conditions (Valentino et al., 2020). This result can be explained by the low uniformity of the system which affects the structure of the film (Perone et al., 2014a). This result agrees with Galus et al. (2020) who reported that the carnauba or candelilla wax dispersed in 8% of SC at a concentration of 0.5% or 1% did not significantly affect the WVP of the film that assumed values ranged from $3.66 \pm 0.12 \times 10^{-10}$ to $2.66 \pm 0.27 \times 10^{-10} \text{ g m}^{-1} \text{ sec}^{-1} \text{ Pa}^{-1}$ at 50% of RH. Sample 12 showed higher WVP than sample 10, even if it has a higher concentration of BW. This can be justified by the more difficult dispersion of the BW in a system with a high GG concentration. This result agrees with Avena-Bustillos and Krochta (1993) who found that the BW was able to reduce the water vapor permeability of a caseinate dispersion up to a concentration of 2% because for higher concentration it was difficult to disperse the BW into the caseinate dispersion. Nandi and Guha (2018) showed that WVP of the film obtained by potato starch and GG increased with guar gum and glycerol content. The authors justified the results considering the hydrophilic nature of guar gum, which facilitated the water molecules to make bonds with the active site of the polymer chain and thus, created microcavities. However, as reported by Alizadeh-Sani et al. (2020), when SC is blended with GG, the WVP of the obtained films decreases as a function of SC concentration, due to the decrease in the free volume and the resulting reduction of water vapor diffusion in the blended system. However, for an emulsion system, WVP is influenced by the interaction between components. Our result showed that the lowest values of WVP were obtained with formulations 10 and 11, which have 1% and 2% of BW and 0.4% and 0.2% of GG, respectively.

3.2.3. Adsorption isotherm

The moisture adsorption isotherms of films obtained from samples 9, 10, 11, and 12 are reported in Fig. 4. All curves showed a sigmoidal shape, characteristic of type III isotherms, which are typical of most biopolymer materials (Fabra et al., 2010; Muscat et al., 2013; Volpe et al., 2017). This type of isotherm absorbs low amounts of water at low

a_w and higher amounts of water at high a_w . The adsorption of water takes place in the monolayer zone at $a_w < 0.2$. In the a_w region between 0.2 and 0.65, the water is absorbed in the multilayer; at $a_w > 0.65$ the water absorbed corresponds to the condensation of water in the pores of the film. Samples 9 and 10 showed the highest amount of water absorbed at 0.95 a_w with a moisture content value of $0.64 \text{ g}_{\text{water}}\text{g}_{\text{dryfilm}}^{-1}$ and $0.62 \text{ g}_{\text{water}}\text{g}_{\text{dryfilm}}^{-1}$ respectively, whereas samples 11 and 12 assumed moisture content values of $0.52 \text{ g}_{\text{water}}\text{g}_{\text{dryfilm}}^{-1}$ and $0.55 \text{ g}_{\text{water}}\text{g}_{\text{dryfilm}}^{-1}$, respectively. In Table 5 GAB model parameters are shown. The value x_m corresponds to the moisture content in the monolayer; it is evidence of the quantity of water that can be bound to a single layer per gram of dry film. The lowest monolayer values were obtained for samples 11 and 12 (0.047 and $0.049 \text{ g}_{\text{water}}\text{g}_{\text{dryfilm}}^{-1}$, respectively) while the highest values were observed for samples 9 and 10 ($0.055 \text{ g}_{\text{water}}\text{g}_{\text{dryfilm}}^{-1}$ and $0.053 \text{ g}_{\text{water}}\text{g}_{\text{dryfilm}}^{-1}$, respectively). The increase in the monolayer moisture content could be attributable to the greater number of sites available for water adsorption; this result may be related to the low concentrations of BW in samples 9 and 10 compared to 11 and 12, which lead to the change in the overall hydrophobicity of the matrix. The sorption energy constant C is related to the measure of the strength of binding of water to the monolayer. The larger C, the stronger the water-substrate interaction is in the monolayer, and the larger the difference in enthalpy between the monolayer molecules and multilayer molecules (Cui et al., 2020; Fabra et al., 2010). It seems that for sample 9 the water-substrate interaction is slightly stronger in the monolayer. The parameter k is related to the heat of the multilayer sorption; when it is close to one, there is no distinction between the molecules in the monolayer and liquid molecules (Quirijns et al., 2005). In our results, constant k approached 1 for all the samples. C and k parameters were in the same range as the value reported by Villalobos et al. (2006) for HPMC films containing surfactant mixtures of sorbitan monostearate and sucrose palmitate. Overall, the presence of lipids allowed to reduce the water sorption since the beeswax corresponds to a fraction of solid with small uptake of water. These results agree with Fabra et al. (2010) that found that BW seemed to inhibit the water sorption capacity of the sodium caseinate matrix probably due to the promotion of hydrophobic interactions between lipid and protein. In our case the amount of BW (1% or 2%), affected the water sorption; indeed, formulations 11 and 12 showed lower water absorbed at the equilibrium state compared to formulations 9 and 10, most likely due to the higher concentration of BW (2%). With the same amount of BW, the GG concentration seemed to promote the water binding, due to a large number of hydrophilic groups present in their structure. Based on the above results, sample 11 was selected as the one with the best properties in terms of stability, PSD, and WVP.

3.3. Coating thickness, transpiration and respiration rates of strawberries

The average liquid thickness (h_{avg}) and the dry coating thickness estimated on strawberries (H_{avg}) were found to be $63 \pm 8 \mu\text{m}$ and $4,5 \pm 0.6 \mu\text{m}$, respectively. Valentino et al. (2020) reported that for SC at 8%, the average dry coating thickness on fennel was $2 \mu\text{m}$. Thus, blending sodium caseinate with other polymers, allowed to increase the viscosity of the solution and the thickness of the coating on the product. The thickness of the coating on the fruits depends also on the wettability of the coating solution on the fruits (Park, 1999). As reported by Ribeiro

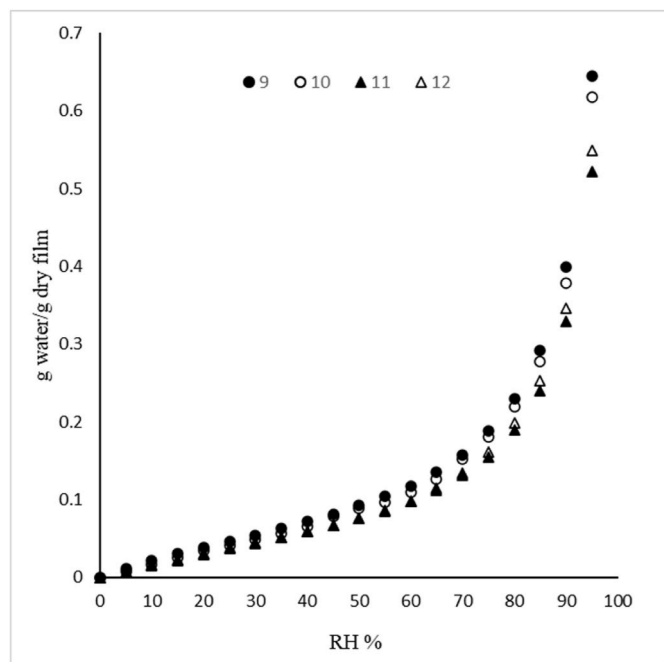


Fig. 4. Equilibrium moisture sorption isotherm for films obtained from formulations 9, 10, 11 and 12.

Table 5
GAB Estimated model constant for films obtained from samples 9, 10 11 and 12.

Model parameters	Samples			
	9	10	11	12
m_0	0.055	0.053	0.047	0.049
C	5.8	4.9	5.1	4.3
k	0.964	0.964	0.960	0.961
RMSE	0.205	0.330	0.156	0.148
R^2	0.9998	0.9995	0.9998	0.9999

et al. (2007), because the strawberry surface is very irregular, the wettability is optimized for liquids with a contact angle below 90° , that is for hydrophilic material. Thus, the results showed that due to the hydrophilic nature of the coating and the viscosity of the solution, the solution was able to form a thin layer of film on the product.

The transpiration rate results are shown in Fig. 5a. In all experimental conditions, the weight of strawberries decreased over time for all the samples; TR ranged from 0.03 to $0.09 \text{ g kg}^{-1} \text{ h}^{-1}$ overall the combinations of RH studied. Higher values were found at 76% of RH, equal to 0.09 ± 0.02 and $0.07 \pm 0.01 \text{ g kg}^{-1} \text{ h}^{-1}$, for the control and coated sample, respectively. At 76% RH, no differences were observed between the coated and uncoated samples. By increasing the RH to 86% and 96% the coating was able to reduce the TR by about 40% and 50%, respectively. Thus, when strawberries are stored at relative humidity higher than 86%, the coating provides a semipermeable layer, able to restrict the moisture transfer from the interior of the strawberry to the environment.

These values of TRs of strawberries are much lower than those found by Sousa-Gallagher et al. (2013) for single uncoated strawberry, having a range of $0.24\text{--}0.7 \text{ g kg}^{-1} \text{ h}^{-1}$ at 5°C at the same range of RH, and by Bovi et al. (2018) which reported TR values ranged from 0.13 to $0.7 \text{ g kg}^{-1} \text{ h}^{-1}$ at 4°C at the same range of RH. The differences in TR because the TR is a phenomenon product or commodity-dependent; in fact, it is affected by several factors, such as maturity stage, cultivar, the surface to volume ratio, morphological characteristics etc. The respiration rate results are shown in Fig. 5b. The uncoated and coated samples showed consumption of O_2 of $46 \pm 3 \text{ ml kg}^{-1} \text{ h}^{-1}$ and $38 \pm 3 \text{ ml kg}^{-1} \text{ h}^{-1}$, respectively. Thus, the coating was able to reduce the respiration rate of strawberries by 17%. Velickova et al. (2013) reported that the addition of beeswax in the chitosan biopolymer, as a separate layer or as a component of the composite coating, significantly reduced the respiration rate and weight loss of strawberries. It is important to consider that also respiration may impact water loss. Indeed, respiration produces metabolic heat, which can increase the water lost in transpiration (Volpe et al., 2018; Rux et al., 2015). For most commodities a weight loss of 3–10% is not acceptable, because the product loses its marketability; for strawberries, the water loss at which the product becomes unsalable is 6% (Ben-Yehoshua et al., 1998). Thus, the coating should avoid an excessive water loss, which leads to a reduction in the shelf life. This can be obtained by reducing the transpiration rate.

4. Conclusion

The caseinate-based coating formulation can be properly optimized

by blending it with guar gum and beeswax. Optimization of coating composition required a deep investigation of the physical properties of the dispersion system and the obtained film to reach the required coating properties. Emulsifiers were needed to assure coating stability and HLB played a fundamental role in the stability as well as uniformity and size of the lipid phase in the film-forming blends, by using the same emulsion preparation process. Thus, the HLB has to be properly chosen for the type of lipid and the composition of the film-forming blend. In our case, an HLB of 9.2 was necessary to obtain stable formulations with small beeswax particles, uniformly distributed, and an adequate viscosity. Moreover, only the formulation contained 8% SC, 0.2% GG, and 2% BW showed the lowest hydrophilicity and highest barrier property against water vapor. The optimized coating reduced transpiration and respiration rate of strawberries by 40% and 17%, respectively, at 4°C and high relative humidity (>86%).

Funding

This work was supported by European Union's H2020 Research and Innovation Program (No.817936).

Authorship

All persons who meet authorship criteria are listed as authors, and all authors certify that they have participated sufficiently in the work to take public responsibility for the content, including participation in the concept, design, analysis, writing, or revision of the manuscript. Furthermore, each author certifies that this material or similar material has not been and will not be submitted to or published in any other publication.

In the table below, indicate the specific contributions made by each author (list the authors' initials followed by their surnames, e.g., Y.L. Chang) to the submitted manuscript. A check mark (x) must appear against the name of each author at least once in each of the three categories below.

N.A. Miele: Acquisition of data, Data analysis and/or interpretation, Drafting of manuscript and/or critical revision. S. Volpe: Acquisition of data, Data analysis and/or interpretation, Drafting of manuscript and/or critical revision. S. Cavella: Conception and design of study, Data analysis and/or interpretation, Drafting of manuscript and/or critical revision, Approval of final version of manuscript. E. Torrieri: Conception and design of study, Data analysis and/or interpretation, Drafting of manuscript and/or critical revision, Approval of final version of manuscript.

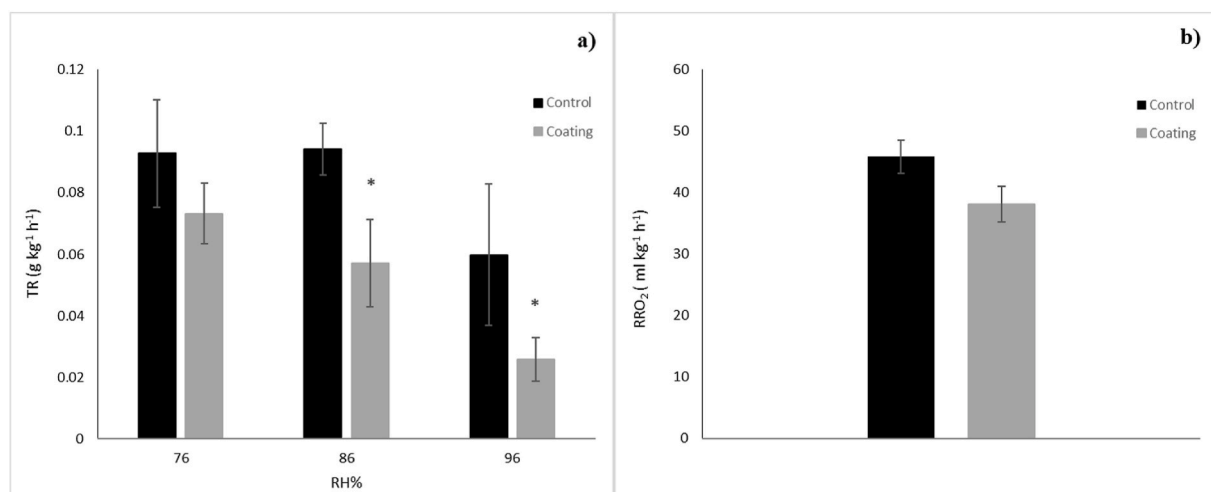


Fig. 5. Transpiration rate of coated and control strawberries expressed in $\text{g kg}^{-1} \text{ h}^{-1}$ at 4°C and 75%, 86% and 96% RH (a). Respiration rate of coated and control strawberries expressed as RRO_2 ($\text{ml kg}^{-1} \text{ h}^{-1}$) calculated at 4°C (b).

Declaration of competing interest

The authors declare no conflict of interest.

References

- Alizadeh-Sani, M., Rhim, J.W., Azizi-Lalabadi, M., Hemmati-Dinarvand, M., Ehsani, A., 2020. Preparation and characterization of functional sodium caseinate/guar gum/TiO₂/cumin essential oil composite film. *Int. J. Biol. Macromol.* 145, 835–844. <https://doi.org/10.1016/j.jbiomac.2019.11.004>.
- Avena-Bustillos, R.J., Krochta, J.M., 1993. Water vapor permeability of caseinate-based edible films as affected by pH, calcium crosslinking and lipid content. *J. Food Sci.* 58 (4), 904–907. <https://doi.org/10.1111/j.1365-2621.1993.tb09388.x>.
- Ben-Yehoshua, S., Rodov, V., Fishman, S., Peretz, J., 1998. Modified-atmosphere packaging of fruits and vegetables: reducing condensation of water in bell peppers and mangoes. *Acta Hortic.* 464, 387–392. <https://doi.org/10.17660/ActaHortic.1998.464.59>.
- Bovi, G.G., Rux, G., Caleb, O.J., Herppich, W.B., Linke, M., Rauh, C., Mahajan, P.V., 2018. Measurement and modelling of transpiration losses in packaged and unpackaged strawberries. *Biosyst. Eng.* 174, 1–9. <https://doi.org/10.1016/j.biosystemseng.2018.06.012>.
- Cavella, S., Miele, N., Fidalgo, M., Borriello, A., Masi, P., 2020. Evolution of particle size distribution, flow behaviour and stability during mill ball refining of a white chocolate flavouring paste. *LWT* 132, 109910. <https://doi.org/10.1016/j.lwt.2020.109910>.
- Cisneros-Zevallos, L., Krochta, J.M., 2003. Dependence of coating thickness on viscosity of coating solution applied to fruits and vegetables by dipping method. *J. Food Sci.* 68 (2), 503–510. <https://doi.org/10.1111/j.1365-2621.2003.tb05702.x>.
- Cui, Y., Gao, S., Zhang, R., Cheng, L., Yu, J., 2020. Study on the moisture absorption and thermal properties of hydroscopic exothermic fibers and related interactions with water molecules. *Polymers* 12 (1). <https://doi.org/10.3390/polym12010098>.
- Domian, E., Szczepaniak, M., 2020. Rheological behavior of concentrated emulsions containing carotenoids with different polarity. *J. Food Eng.* 274, 109827. <https://doi.org/10.1016/j.jfoodeng.2019.109827>.
- Espitia, P.J.P., Fuenmayor, C.A., Otoni, C.G., 2019. Nanoemulsions: synthesis, characterization, and application in bio-based active food packaging. *Compr. Rev. Food Sci. Food Saf.* 18 (1), 264–285. <https://doi.org/10.1111/1541-4337.12405>.
- Fabra, M.J., Talens, P., Chiralt, A., 2010. Water sorption isotherms and phase transitions of sodium caseinate-lipid films as affected by lipid interactions. *Food Hydrocolloids* 24 (4), 384–391. <https://doi.org/10.1016/j.foodhyd.2009.11.004>.
- Falguera, V., Quintero, J.P., Jiménez, A., Muñoz, J.A., Ibarz, A., 2011. Edible films and coatings: structures, active functions and trends in their use. *Trends Food Sci. Technol.* 22 (Issue 6), 292–303. <https://doi.org/10.1016/j.tifs.2011.02.004>.
- Fei, T., Leyva-Gutiérrez, F.M.A., Wan, Z., Wang, T., 2021. Development of a novel soy-wax containing emulsion with enhanced antifungal properties for the postharvest treatment of fresh citrus fruit. *LWT - Food Science and Technology* 141, 110878. <https://doi.org/10.1016/j.lwt.2021.110878>.
- Galus, S., Gaouditz, M., Kowalska, H., Debeaufort, F., 2020. Effects of candelilla and carnauba wax incorporation on the functional properties of edible sodium caseinate films. *Int. J. Mol. Sci.* 21 (24), 1–19. <https://doi.org/10.3390/ijms21249349>.
- Galus, S., Kadzinska, J., 2015. Food applications of emulsion-based edible films and coatings. *Trends Food Sci. Technol.* 45, 273–283. <https://doi.org/10.1016/j.tifs.2015.07.011>.
- Giancone, T., Torrieri, E., Pierro, P.D., Mariniello, L., Moresi, M., Porta, R., Masi, P., 2008. Role of constituents on the network formation of hydrocolloid edible films. *J. Food Eng.* 89 (2), 195–203. <https://doi.org/10.1016/j.jfoodeng.2008.04.017>.
- Han, N.S., Basri, M., Rahman, M.B.A., Rahman, R.N.Z.R.A., Salleh, A.B., Ismail, Z., 2011. Phase behavior and formulation of palm oil esters o/w nanoemulsions stabilized by hydrocolloid gums for cosmeceuticals application. *J. Dispersion Sci. Technol.* 32 (10), 1428–1433. <https://doi.org/10.1080/01932691.2010.513301>.
- Hernandez-Izquierdo, V.M., Krochta, J.M., 2008. Thermoplastic processing of proteins for film formation - a review. *J. Food Sci.* 73 (2), 30–39. <https://doi.org/10.1111/j.1750-3841.2007.00636.x>.
- Hong, I.K., Kim, S.I., Lee, S.B., 2018. Effects of HLB value on oil-in-water emulsions: droplet size, rheological behavior, zeta-potential, and creaming index. *J. Ind. Eng. Chem.* 67, 123–131. <https://doi.org/10.1016/j.jiec.2018.06.022>.
- Hopkins, E.J., Chang, C., Lam, R.S.H., Nickerson, M.T., 2015. Effect of flaxseed oil concentration on the performance of a soy protein isolate-based emulsion-type film. *Food Res. Int.* 67, 418–425. <https://doi.org/10.1016/j.foodres.2014.11.040>.
- Jahromi, M., Niakousari, M., Golmakani, M.T., Mohammadifar, M.A., 2020. Physicochemical and structural characterization of sodium caseinate based film-forming solutions and edible films as affected by high methoxyl pectin. *Int. J. Biol. Macromol.* 165, 1949–1959. <https://doi.org/10.1016/j.jbiomac.2020.10.057>.
- Jalali, A., Linke, M., Geyer, M., Mahajan, P.V., 2020. Shelf-life prediction model for strawberry based on respiration and transpiration processes. *Food Packag. Shelf Life* 25, 100525. <https://doi.org/10.1016/j.foodpsl.2020.100525>.
- Khan, M.R., Volpe, S., Valentino, M., Miele, N.A., Cavella, S., Torrieri, E., 2021. Active casein coatings and films for perishable foods: structural properties and shelf-life extension. *Coatings* 11, 899. <https://doi.org/10.3390/coatings11080899>.
- Krstonošić, V., Dokić, L., Nikolić, I., Milanović, M., 2015. Influence of xanthan gum on oil-in-water emulsion characteristics stabilized by OSA starch. *Food Hydrocolloids* 45, 9–17. <https://doi.org/10.1016/j.foodhyd.2014.10.024>.
- Lafarga, T., Colás-Medà, P., Abadías, M., Aguiló-Aguayo, I., Bobo, G., Viñas, I., 2019. Strategies to reduce microbial risk and improve quality of fresh and processed strawberries: a review. *Innovat. Food Sci. Emerg. Technol.* 52, 197–212. <https://doi.org/10.1016/j.ifset.2018.12.012>.
- Lindner, M., Bäumler, M., Stäbler, A., 2018. Inter-correlation among the hydrophilic-lipophilic balance, surfactant system, viscosity, particle size, and stability of candelilla wax-based dispersions. *Coatings* 8, 469. <https://doi.org/10.3390/COATINGS8120469>.
- Ma, X., Chatterton, D.E.W., 2021. Strategies to improve the physical stability of sodium caseinate stabilized emulsions: a literature review. *Food Hydrocolloids* 119, 106853. <https://doi.org/10.1016/j.foodhyd.2021.106853>.
- Martin, M.J., Trujillo, L.A., Garcia, M.C., Alfaro, M.C., Muñoz, J., 2018. Effect of emulsifier HLB and stabilizer addition on the physical stability of thyme essential oil emulsions. *J. Dispersion Sci. Technol.* 39 (11), 1627–1634. <https://doi.org/10.1080/01932691.2018.1459677>.
- McClements, D.J., 2007. Critical review of techniques and methodologies for characterization of emulsion stability. *Crit. Rev. Food Sci. Nutr.* 47 (7), 611–649. <https://doi.org/10.1080/10408390701289292>.
- Muscato, D., Adhikari, R., McKnight, S., Guo, Q., Adhikari, B., 2013. The physicochemical characteristics and hydrophobicity of high amylose starch-glycerol films in the presence of three natural waxes. *J. Food Eng.* 119 (2), 205–219. <https://doi.org/10.1016/j.jfoodeng.2013.05.033>.
- Nandi, S., Guha, P., 2018. Modelling the effect of guar gum on physical, optical, barrier and mechanical properties of potato starch based composite film. *Carbohydr. Polym.* 200, 498–507. <https://doi.org/10.1016/j.carbpol.2018.08.028>.
- Neirynek, N., Van lent, K., Dewettinck, K., Van der Meeren, P., 2007. Influence of pH and biopolymer ratio on sodium caseinate-guar gum interactions in aqueous solutions and in O/W emulsions. *Food Hydrocolloids* 21 (5–6), 862–869. <https://doi.org/10.1016/j.foodhyd.2006.10.003>.
- Otoni, C.G., Avena-Bustillos, R.J., Azeredo, H.M.C., Lorevice, M.V., Moura, M.R., Mattoso, L.H.C., McHugh, T.H., 2017. Recent advances on edible films based on fruits and vegetables—a review. *Compr. Rev. Food Sci. Food Saf.* 16 (5), 1151–1169. <https://doi.org/10.1111/1541-4337.12281>.
- Park, H.J., 1999. Development of advanced edible coatings for fruits. *Trends Food Sci. Technol.* 10 (8), 254–260. [https://doi.org/10.1016/S0924-2244\(00\)00003-0](https://doi.org/10.1016/S0924-2244(00)00003-0).
- Perone, N., Torrieri, E., Nicolai, M.A., Cavella, S., Addeo, F., Masi, P., 2014a. Structure and properties of hydroxypropyl methyl cellulose-sodium caseinate film cross-linked by TGase. *Food Packag. Shelf Life* 1 (2), 113–122.
- Perone, N., Torrieri, E., Cavella, S., Masi, P., 2014b. Effect of rosemary oil and HPMC concentrations on film structure and properties. *Food Bioprocess Technol.* 7 (2), 605–609. <https://doi.org/10.1007/s11947-012-1044-x>.
- Quijirins, E.J., Van Boxtel, A.J.B., Van Loon, W.K.P., Van Straten, G., 2005. Sorption isotherms, GAB parameters and isosteric heat of sorption. *J. Sci. Food Agric.* 85 (11), 1805–1814. <https://doi.org/10.1002/jsfa.2140>.
- Ribeiro, C., Vicente, A.A., Teixeira, J.A., Miranda, C., 2007. Optimization of edible coating composition to retard strawberry fruit senescence. *Postharvest Biol. Technol.* 44 (1), 63–70. <https://doi.org/10.1016/j.postharvbio.2006.11.015>.
- Rux, G., Mahajan, P.V., Geyer, M., Linke, M., Pant, A., Saengerlaub, S., Caleb, O.J., 2015. Application of humidity-regulating tray for packaging of mushrooms. *Postharvest Biol. Technol.* 108, 102–110. <https://doi.org/10.1016/j.postharvbio.2015.06.010>.
- Santos, J., Trujillo-Cayado, L.A., Calero, N., Alfaro, M.C., Muñoz, J., 2016. Development of eco-friendly emulsions produced by microfluidization technique. *J. Ind. Eng. Chem.* 36, 90–95.
- Shamsuri, A.A., Siti Nurul, S.N.A., 2020. Functional properties of biopolymer-based films modified with surfactants: a brief review. *Processes* 8 (9), 1–14. <https://doi.org/10.3390/pr8091039>.
- Sousa-Gallagher, M.J., Mahajan, P.V., Mezdad, T., 2013. Engineering packaging design accounting for transpiration rate: model development and validation with strawberries. *J. Food Eng.* 119 (2), 370–376. <https://doi.org/10.1016/j.jfoodeng.2013.05.041>.
- Sun, X., Wu, Q., Picha, D.H., Ferguson, M.H., Ndukwe, I.E., 2021. Comparative performance of bio-based coatings formulated with cellulose, chitin, and chitosan nanomaterials suitable for fruit preservation. *Carbohydr. Polym.* 259, 117764. <https://doi.org/10.1016/j.carbpol.2021.117764>.
- Valentino, M., Volpe, S., Di Giuseppe, F.A., Cavella, S., Torrieri, E., 2020. Active biopolymer coating based on sodium caseinate: physical characterization and antioxidant activity. *Coatings* 10, 706. <https://doi.org/10.3390/COATINGS10080706>.
- Velickova, E., Winkelhausen, E., Kuzmanova, S., Alves, V.D., Moldão-Martins, M., 2013. Impact of chitosan-beeswax edible coatings on the quality of fresh strawberries (*Fragaria ananassa* cv Camarosa) under commercial storage conditions. *LWT - Food Sci. Technol. (Lebensmittel-Wissenschaft -Technol.)* 52 (2), 80–92. <https://doi.org/10.1016/j.lwt.2013.02.004>.
- Villalobos, R., Hernández-Muñoz, P., Chiralt, A., 2006. Effect of surfactants on water sorption and barrier properties of hydroxypropyl methylcellulose films. *Food Hydrocolloids* 20 (4), 502–509. <https://doi.org/10.1016/j.foodhyd.2005.04.006>.
- Volpe, S., Cavella, S., Masi, P., Torrieri, E., 2017. Effect of solid concentration on structure and properties of chitosan-caseinate blend films. *Food Packag. Shelf Life* 13, 76–84. <https://doi.org/10.1016/j.foodpsl.2017.07.002>.
- Volpe, S., Cavella, S., Torrieri, E., 2019. Biopolymer coatings as alternative to modified atmosphere packaging for shelf life extension of minimally processed apples. *Coatings* 9, 569. <https://doi.org/10.3390/coatings9090569>.
- Volpe, Stefania, Mahajan, P.V., Rux, G., Cavella, S., Torrieri, E., 2018. Condensation and moisture regulation in packaged fresh-cut iceberg lettuce. *J. Food Eng.* 216, 132–137. <https://doi.org/10.1016/j.jfoodeng.2017.08.015>.
- Zhang, W., Qin, Y., Gao, Z., Ou, W., Zhu, H., Zhang, Q., 2019. Phase behavior and stability of nano-emulsions prepared by D phase emulsification method. *J. Mol. Liq.* 285, 424–429. <https://doi.org/10.1016/j.molliq.2019.04.112>.